Adipocyte deletion of the RNA binding protein HuR induces cardiac hypertrophy and fibrosis

Adrienne R. Guarnieri[1], Sarah R. Anthony[1], Anamarie Gozdiff[1], Lisa C. Green[1], Sam Slone[1], Michelle L. Nieman[2], Perwez Alam[3], Joshua B. Benoit[4], Onur Kanisicak[3], Michael Tranter[1*]

[1] Department of Internal Medicine, Division of Cardiovascular Health and Disease, University of Cincinnati College of Medicine, Cincinnati, OH

[2] Department of Pharmacology & Systems Physiology, University of Cincinnati College of Medicine, Cincinnati, OH

[3] Department of Pathology and Laboratory Medicine, University of Cincinnati College of Medicine, Cincinnati, OH

[4] Department of Biological Sciences, University of Cincinnati, Cincinnati, OH

Running Title: Adipocyte-specific HuR deletion mediates CVD

[*] Correspondence: Michael Tranter, PhD
Division of Cardiovascular Health and Disease
Department of Internal Medicine
University of Cincinnati College of Medicine
231 Albert Sabin Way, CVC 3928
Cincinnati, OH 45267
Michael.Tranter@UC.edu
513-558-3507

Keywords: Cardiovascular Disease, Cardiac hypertrophy, fibrosis, adipose tissue, HuR

ABSTRACT

Adipose tissue continues to gain appreciation for its broad role as an endocrine organ, and disruptions in adipose tissue homeostasis plays a central role in cardiovascular physiology. We have previously shown that expression of the RNA binding protein HuR in adipose tissue mediates energy expenditure, but the potential cardiovascular impacts of this finding have not been explored. We show here that adipose tissue-specific deletion of HuR (Adipo-HuR$^{-/-}$) is sufficient to induce the spontaneous development of cardiac hypertrophy and fibrosis. Hearts from Adipo-HuR$^{-/-}$ mice have increased left ventricular (LV) ejection fraction, rate of pressure generation, and LV posterior wall thickness that is accompanied by an increase in LV/body weight ratio and hypertrophic gene expression. Furthermore, Adipo-HuR$^{-/-}$ hearts display increased fibrosis by picrosirius red staining and periostin expression. To identify underlying mechanisms, we applied both RNA-seq and weighted gene co-expression network analysis (WGCNA) to define HuR-dependent changes in gene expression as well as significant relationships between adipose tissue gene expression and LV mass. RNA-seq results demonstrate a significant increase in pro-inflammatory gene expression in the subcutaneous white adipose tissue (scWAT) from Adipo-HuR$^{-/-}$ mice that is accompanied by an increase in serum levels of both TNF-α and IL-6. WGCNA identified a significant enrichment in inflammation, apoptosis/cell death, and vesicle-mediated transport genes among those whose expression most significantly associated with CVD in Adipo-HuR$^{-/-}$. In conclusion, we demonstrate that the loss of HuR expression in adipose tissue promotes the development of cardiac hypertrophy and fibrosis, potentially through modulation of inflammation and vesicle-mediated transport in scWAT.

NEW AND NOTEWORTHY

This work demonstrates the spontaneous development of cardiac hypertrophy and fibrosis upon adipose tissue-specific deletion of the RNA binding protein HuR that appears to be mechanistically driven by HuR-dependent changes in inflammatory and extracellular vesicle transport mediating genes in the subcutaneous white adipose tissue. These results suggest that loss of HuR expression in adipose tissue in obesity, as demonstrated in mouse and humans by our group and others, may contribute to obesity-mediated CVD.

INTRODUCTION

Obesity and metabolic syndrome are known co-morbidities of cardiovascular disease (CVD), and as the prevalence of obesity in the U.S. continues to climb, understanding of the causal relationship between disruption in adipose tissue homeostasis and CVD is of critical significance. Obesity and metabolic syndrome are both driven by imbalances in energy consumption, storage, and expenditure, and are marked by an increase in lipid storage and disruption of adipose tissue homeostasis. When energy intake exceeds expenditure, excess caloric energy is stored in white adipose tissue (WAT) as triglycerides. In contrast, beige and brown adipose tissue (BAT) drive energy expenditure through uncoupled thermogenic metabolism in their conserved evolutionary role in thermoregulation. Functional BAT, previously only believed to be in infants and children, was recently discovered in adult humans (12, 80) and is considered a potential therapeutic target in obesity due to its high metabolic potential, which is capable of accounting for up to 20% of total whole-body energy expenditure (65, 75, 76).

Adipose tissue has long been linked to CVD through its central role in obesity, but work over the past two decades has established a clear endocrine organ role for adipose tissue that is dependent on both adipocyte composition (e.g. WAT vs. BAT) as well as anatomical location (e.g. visceral vs. subcutaneous) (2). Specifically, accumulation of WAT tends to be more pro-inflammatory in nature, especially under conditions of chronic energy surplus, and exerts deleterious effects on cardiovascular health (19, 55, 59). On the other hand, the presence of metabolically active BAT has been demonstrated to positively correlate with myocardial health (2, 63, 72, 74).

Human antigen R (HuR) is a widely-expressed RNA binding protein that interacts with specific AU-rich domains in target mRNAs and directly regulates expression by modulating mRNA stability and/or translation (14). Our recently published work was among the first to show the *in vivo* role of HuR on adipocyte physiology (1). Two other groups have also recently shown roles for HuR in adipogenesis and lipolysis (48, 69). We specifically showed that adipocyte-specific deletion of HuR in mice (Adipo-HuR$^{-/-}$ mice) resulted in a reduction in both WAT and BAT mass that was accompanied by a profound

deficit in adaptive thermogenesis when subjected to acute cold challenge (1). Interestingly, Li et al recently showed an inverse correlation between HuR expression in subcutaneous WAT (scWAT) and obesity in human patients (48), suggesting a clinical link for HuR expression in metabolic syndrome and raising the question as to whether loss of HuR expression in adipose tissue may play a functional role in obesity associated co-morbidities such as CVD. Prior to showing a role for HuR in adipocyte function, we independently demonstrated a role for HuR expression in cardiomyocytes during the progression of pathological cardiac hypertophy (24, 70). However, in light of the growing interest in the adipose tissue-to-myocardium signaling axis, potential HuR-mediated cross-talk between adipose tissue and the myocardium has not yet been explored.

Here, we demonstrate that adipocyte-specific deletion of HuR mediates the spontaneous development of left ventricular cardiac hypertrophy and fibrosis in mice that appears to be mechanistically driven by an increase in inflammatory gene expression in subcutaneous white adipose tissue.

MATERIALS AND METHODS

Animal Models. All mouse studies were approved by the University of Cincinnati Institutional Animal Care and Use Committee (IACUC). HuR floxed mice were described by Ghosh et al (22) and obtained from Jackson Labs (stock # 021431). To generate an adipose-specific HuR deletion model (*Adipo-HuR*$^{-/-}$), HuR-floxed mice were crossed with mice harboring an adiponectin-specific Cre recombinase transgene (*AdipoQ-Cre*) (Jackson Labs, stock # 010803). Non-floxed *Adipo-cre*$^{+}$ littermates were used as controls. Mice were housed in the University of Cincinnati vivarium at 23^{o}C. All data presented is from 18-22 week old male mice.

Echocardiography. All echocardiographic studies were performed as previously described (24). Briefly, mice were sedated with isoflurane and body temperature was maintained at 37^{o}C during imaging. Using a Vevo 2100, parasternal images were obtained in long axis in two-dimensional mode and motion (M)-mode for quantification. These were then analyzed using VevoStrain software (Vevo 2100, v1.1.1 B1455, Visualsonic, Toronto, Canada).

LV Pressure Catheterization. As a terminal procedure, mice were weighed and anesthetized using inhaled isoflurane. Terminal development of LV pressure was determined using a 1.2-French catheter pressure transducer (Scisense FTH-1211B-0018) advanced through the carotid into the LV as previously described (17, 51).

Tissue and plasma processing. At time of euthanasia, mice were sedated with isoflurane and blood collected into 3.2% sodium citrate to collect plasma via centrifugation at 4,000 x g at room temperature, which was snap frozen. Mice were subsequently euthanized via thoracotomy and tissues were removed, weighed, and flash frozen in liquid nitrogen for further analysis. Plasma catecholamine (epinephrine, norepinephrine; Abnova KA1877), IL-6 (Bioss BSKM1004) and TNF-α (Bioss BSKM1002) levels were assessed using ELISA kits according to the manufacturers' instructions.

Histological Analysis. Frozen hearts were embedded in OCT, sectioned, and stained using Picrosirius red (Polysciences, Inc) as previously described (29). Briefly, slides were air dried, immersed in xylene for 10 minutes, and hydrated through decreasing concentrations of ethanol (100%, 96%, 80% and 70%, 10 seconds each). They were then stained according to the manufacturer's instructions, dehydrated through increasing concentrations of ethanol, cleared in xylene, and mounted with Permount under a glass coverslip.

RNA Isolation and qPCR. RNA was isolated using a Macherey-Nagel NucleoSpin RNA kit and cDNA was synthesized using iScript RT Supermix (Bio-Rad). Samples were run on a Bio-Rad CFX96 Touch to assess mRNA levels of BNP, RCAN, and 18S. Primers are as listed: BNP, F: 5'-AAGTCCTAGCCAGTCTCCAGA-3', R: 5'-GAGCTGTCTCTGGGCCATTTC-3'; RCAN, F: 5′-GGGCCAAATTTGAATCCCTCTTC-3′, R: 5′-GGAGCCAGGTGTGAACTTCC-3′; 18S, F: 5'-AGTCCCTGCCCTTTGTACACA-3', R: 5'-CCGAGGGCCTCACTAAACC-3'.

Protein Isolation and Western blotting. Total protein was isolated from crushed tissue in RIPA buffer with 0.5 mM DTT, 0.2 mM sodium-orthovanadate, and a protease inhibitor mixture tablet (Complete mini; Roche Applied Science). 25 ug of protein extract per lane was separated on a 10% polyacrylamide gel and transferred to a nitrocellulose membrane. Blocking was performed for 1 h at room temperature using 5% BSA milk in 0.1% Tween 20, tris-buffered saline (T-TBS). Primary antibodies for Periostin (Novus Biologicals NBP1-30042), PERK (Cell Signaling, 3192), and GAPDH (Santa Cruz Biotechnology sc25778) were incubated overnight at 4°C, and secondary antibodies were incubated for 1–2 h at room temperature in T-TBS. Images were captured and analyzed using a ChemiDoc Imaging System and ImageLab software (BioRad).

RNA Sequencing and Weighted Gene Co-Expression Network Analysis (WGCNA). RNA was isolated from cardiac and adipose tissue as previously described (1, 70) and RNA sequencing was done by the Cincinnati Children's Hospital Medical Center (CCHMC) DNA Sequencing and Genotyping

Core. Sequence read mapping, principal component analysis, and differential expression analysis was done using CLC Genomics Workbench (v. 20.0.2, Qiagen) as previously described (1, 24). Gene ontology analysis was done using the NIH DAVID Bioinformatics Functional Annotation Tool with an EASE score/P-value threshold of 0.05 as previously described (35, 36, 77). Significant differential expression between groups was defined as an absolute fold change of greater than or equal to 1.5 and a false discovery rate adjusted (FDR) p-value of less than or equal to 0.05. For WGCNA, co-expression network construction, module detection, association of expression modules with phenotype data, and identification of node genes withing expression modules was done as previously described (46, 89). Node genes were defined as the top 10 genes with the highest sum of absolute module membership and gene significance values and a gene significance value of > 0.85. All RNA-seq data is available in the NCBI Gene Expression Omnibus (https://www.ncbi.nlm.nih.gov/geo/) (GDSXXX).

RESULTS

Cardiac function in Adipo-HuR$^{-/-}$ mice. Examination of cardiac function in 20-week old mice by echocardiography showed an increase in left ventricular (LV) ejection fraction (Fig. 1A), decreased LV volume at systole (along with a strong trend to decrease in diastole; Figs. 1B-C), and increased LV posterior wall thickness (Fig. 1D) in hearts from Adipo-HuR$^{-/-}$ mice compared to littermate controls. Invasive hemodynamic assessment via LV pressure catheterization also shows an increased rate of positive and negative pressure generation in Adipo-HuR$^{-/-}$ hearts (Fig. 1E-F). As we have previously shown a decrease in body weight in Adipo-HuR$^{-/-}$ mice (1), cardiac structural changes have been normalized to body weight. Together, these data are indicative of a state of compensated cardiac hypertrophy in Adipo-HuR$^{-/-}$ mice.

Molecular assessment of cardiac hypertrophy and fibrosis. First, LV mass relative to body mass was found to be significantly increased in Adipo-HuR$^{-/-}$ mice (Fig. 2A), and qPCR showed increased expression of the hypertrophic marker genes BNP and RCAN (Fig. 2B-C). Next, assessment of cardiac fibrosis via picrosirius red collagen staining found increased interstitial fibrosis throughout the myocardium of Adipo-HuR$^{-/-}$ mice (Fig. 2D-E). This was accompanied by a significant increase in protein expression of periostin, a marker for active myofibroblast ECM remodeling, and the ER-stress marker PERK (Fig. 2F-H). Thus, molecular signaling within the myocardium was found to be consistent with pathological hypertrophy.

Circulating catecholamine levels. Adrenergic signaling response to cold activates thermogenic pathways, but also mediates increased cardiac contractility upon acute exposure and pathological cardiac hypertrophy with prolonged exposure (18). Thus, to rule out adrenergic-induced cardiac pathology as a result of cold-intolerance in Adipo-HuR$^{-/-}$ mice, we show that plasma levels of epinephrine and norepinephrine are not increased (Fig. 3A and B, respectively). This demonstrates that the cardiac hypertrophy and fibrosis observed in Adipo-HuR$^{-/-}$ mice is not driven by increased adrenergic signaling.

RNA-seq assessment of cardiac gene expression. Transcriptome-wide RNA-sequencing was used to identify the full breadth of cardiac gene expression changes upon HuR deletion in adipose tissue. Principal component analysis showed a clear distinction between cardiac transcriptomes in Adipo-HuR$^{-/-}$ mice and littermate controls (Fig. 4A). We identified a total of 476 significantly dysregulated genes, as defined by a fold change of ≥ 1.5 and a false discover rate (FDR)-corrected *P* value of ≤ 0.05. Of these significant genes, 218 were significantly down-regulated and 258 were significantly up-regulated relative to expression in control hearts. Gene ontology (GO) analysis identified a significant enrichment in GO terms for inflammatory gene expression among significantly upregulated genes in hearts from Adipo-HuR$^{-/-}$ mice (Fig. 4B). In addition to an increase in many individual pro-inflammatory genes, RNA-seq analysis also confirmed a significant increase in pro-fibrotic and hypertrophic genes (Fig. 4C).

RNA-seq assessment of adipose tissue gene expression. We previously reported RNA-seq analysis of HuR-dependent changes in BAT (1), but found nothing that would be obviously indicative of cardiovascular disease. Here, we again applied RNA-seq (with a statistical cutoff of a fold change of ≥ 1.5 and an FDR *P* value of ≤ 0.05) to identify transcriptome-wide HuR-dependent gene expression in scWAT. Results show that while HuR mediates expression of 588 genes in BAT, we found 1117 HuR-dependent genes in scWAT (Fig. 5A). Interestingly, many of the HuR-dependent gene expression changes in BAT were decreases in expression, but most HuR-dependent changes in scWAT were increases in expression, suggesting differing roles for HuR-mediated gene expression in the two tissues (Fig. 5B).

Among the significant gene expression changes in scWAT, we observe an increase in many pro-thermogenic genes/beige adipocyte markers (Fig. 5C), which is not surprising given thermogenic deficiency previously reported in Adipo-HuR$^{-/-}$ mice (1). Gene ontology (GO) analysis of HuR-dependent gene expression changes in scWAT show an overwhelming enrichment in pro-inflammatory mediators, as ~33% of all significant GO terms are associated with inflammation/immune processes

(Fig. 5D). Many of the top 20 enriched GO terms among HuR-dependent up-regulated genes in scWAT are inflammation associated GO terms (Fig. 5E). Among these increased inflammatory gene products are several pro-inflammatory cytokines which play a detrimental role in cardiac physiology (Fig. 5F) (13, 21, 26, 73). Importantly, we also show an increase in plasma levels of TNF-α and IL-6 (Fig. 5G and 5H, respectively), suggesting that this large increase in inflammatory gene expression in scWAT results in an increase in systemic inflammation.

Association of adipose tissue expression networks with cardiac phenotype. To more specifically determine which gene expression changes within the scWAT are likely to underlie specific pathological changes in the heart, we applied weighted gene co-expression network analysis (WGCNA) (46, 89). Here, we applied WGCNA analysis to cluster the scWAT transcriptome into co-expressed gene modules, then associate each module with cardiac phenotype through a parallel analysis of module-phenotype correlation and average module eigengene significance within each module (Fig. 6A). After clustering the scWAT transcriptome into co-expressed gene modules independent of genotype (Fig. 6B), cardiac hypertrophy (left ventricle weight to body weight ratio; LVW/BW) was used as the specific cardiac phenotype of interest to identify scWAT gene expression associations. We identified three significant co-expression modules (*lightsteelblue1, magenta,* and *yellowgreen*) that passed criteria for both module-phenotype correlation ($P \leq 0.05$; Fig. 6C) and average gene significance (0.75) relative to LV/BW (Fig. 6D). Overall significance of these modules was confirmed through linear correlation demonstrating a strong relationship between individual gene significance to phenotype and module membership (Fig. 6E).

Subsequent Gene ontology analysis of individual genes within these three co-expression modules revealed a significant enrichment for genes associated with apoptosis/cell death and vesicle mediated transport (Figure 7). Within each module, individual node genes, or those that have the highest gene significance and module membership score within each module, can be identified as those genes that have the highest likelihood of having a causal relationship with the phenotype. Congruent with the GO results, the majority of these node genes play a significant role in either inflammation, apoptosis, or

vesicular mediated transport. A full list of these node genes, their individual association with LVW/BW, and relevant biological functions are found in Table 1. The association of apoptosis-related co-expression modules in scWAT with cardiac pathology is consistent with the inflammatory phenotype observed in both tissues, but these results also suggest paracrine signaling via extracellular vesicles as a potential mediator of scWAT-derived mediator of pathological cardiac hypertrophy.

DISCUSSION

In this work, we demonstrate that hearts from Adipo-HuR$^{-/-}$ mice develop cardiac hypertrophy with increased LV/BW ratio, LV wall thickness, and increase in hypertrophic marker genes. These mice also show an increase in cardiac fibrosis with increased expression of fibrotic (periostin) and ER stress (PERK) proteins. Increased PERK expression indicates activation of the unfolded protein response (UPR) and ER stress, which has been shown to be induced in multiple forms of CVD and is increased in failing human hearts (37, 90). Consistent with these results, RNA-seq analysis also shows a broad increase in hypertrophic, fibrotic, and inflammatory marker genes in these hearts confirming pathological hypertrophy and fibrosis. Perhaps most significant is that the cardiovascular pathology described in Adipo-HuR$^{-/-}$ mice is driven via adipocyte-specific signaling in the absence of glucose intolerance, changes in circulating lipid levels, or obesity (all data presented are from lean mice maintained on control chow diet). We have previously shown that Adipo-HuR$^{-/-}$ mice have no differences in glucose tolerance or plasma phospholipids, cholesterol, triglycerides, or non-esterified fatty acids (1).

Both scWAT inflammation and BAT dysfunction have been previously associated with CVD through disparate independent mechanisms (2). In our prior work, we demonstrated the role of adipocyte-specific HuR deletion on the function of BAT, including a full RNA-seq analysis of HuR-dependent gene expression in BAT (1), but found nothing that would suggest a CVD-mediating effect emanating from direct HuR-dependent changes in BAT. However, data presented here shows a large degree of gene expression in scWAT that appears to be the result of direct compensation for the loss of BAT-mediated thermogenesis. Indeed, many gene markers of thermogenesis suggesting the beiging of scWAT, such as *ucp1*, *elovl3*, and *cidea*, are significantly increased in scWAT from Adipo-HuR$^{-/-}$ mice. Interestingly though, the majority of gene expression changes in scWAT, as categorized by gene ontology analysis, were associated with immune and inflammatory processes. This increased inflammatory gene expression in scWAT is accompanied by a systemic increase in circulating IL-6 and TNF-α, both of which have been shown to mediate CVD (26, 56, 92).

To expand upon the standard RNA-seq analysis and identify potentially unique gene expression changes within the scWAT that are likely to underlie specific pathological changes in the heart, we applied weighted gene co-expression network analysis (WGCNA) (46, 89). WGCNA has been shown to be a powerful tool to directly correlate gene expression changes with phenotype and is an excellent predictor of causal relationships (28, 81, 83). Gene ontology analysis of individual genes within co-expressed gene modules showing a positive association with cardiac hypertrophy revealed two central themes: apoptosis/cell death and vesicle mediated transport. The association of apoptosis/cell death genes with hypertrophy would appear to further support a role for the increase in inflammatory genes identified herein. The identification of vesicle-mediated transport enriched genes is an intriguing potential mechanism for scWAT-mediated paracrine signaling to the myocardium. Future work will be needed to fully define whether increased inflammation or dysregulation of vesicular-mediated transport (or both) from scWAT is driving the phenotype seen in this model and to what extent these mechanisms play a broader role in the adipose-myocardial signaling axis.

The potential translational impact of decreased HuR expression in adipose tissue and its impact on CVD remain to be fully elucidated. Indeed, we observe a decrease in HuR expression in scWAT from obese wild-type mice, confirming the previously published report of decreased HuR expression in scWAT from obese humans (48). Here, we show that loss of HuR expression in adipose tissue is sufficient to induce CVD in the absence of obesity, but a direct mechanistic role for decreased adipose tissue expression of HuR in promoting CVD in humans remains unexplored. Future work will be needed to address this and other remaining questions. For example, HuR has been previously shown to be a mediator of inflammatory signaling (27, 42, 44, 71, 87), but the specific mechanisms by which loss of HuR expression in scWAT drives inflammatory signaling remains unknown. Furthermore, are scWAT-mediated increases in inflammatory mediators, such as TNF-α and IL-6 as we have shown here, sufficient to induce the observed CVD and to what extent might scWAT-derived extracellular vesicles signal to the myocardium? Another important remaining question is whether the loss of BAT-

mediated thermogenesis directly contributes to the CVD observed in our model. An inverse clinical correlation between CVD and functional declines in BAT associated with aging, obesity, and other CVD co-morbidities has been noted, but the loss of functional BAT has yet to be conclusively shown to play a direct causal role in CVD.

GRANTS

This work was partially supported by an American Heart Association Transformational Project Award (19TPA34910086; MT) and NIH grant R01 HL132111 (MT). LCG and SS are supported by AHA Predoctoral Fellowships (20PRE35210795 and 20PRE35230020, respectively).

DISCLOSURES

The authors report no conflicts of interest, financial or otherwise.

AUTHOR CONTRIBUTIONS

A.R.G., S.R.A., A.G., and M.T. conceived and designed the research. A.R.G., S.R.A., A.G., L.C.G., S.S., M.L.N., P.A., and M.T. performed experiments and analyzed data. A.R.G., S.R.A., A.G., J.B.B., O.K., and M.T. interpreted results. A.R.G., S.R.A., and M.T. drafted, edited, and revised the manuscript.

FIGURE LEGENDS

Figure 1. Functional assessment of cardiac function in hearts from mice with an adipocyte-specific deletion of HuR. Echocardiographic analysis shows that hearts from Adipo-HuR$^{-/-}$ mice have increased %EF (A), with decreased LV chamber volume (B-C), and increased LV posterior wall thickness (D). LV pressure catheterization shows an exacerbation in the rates of positive and negative developed pressure (E-F). n ≥ 4 per group. *P ≤ 0.05; ** P ≤ 0.01.

Figure 2. Molecular assessment of cardiac hypertrophy and fibrosis. Adipo-HuR$^{-/-}$ have increased ventricle weight to body weight ratios compared to control mice (A). Gene expression of the hypertrophic markers BNP and RCAN were also increased in Adipo-HuR$^{-/-}$ mice (B, C). Hearts from Adipo-HuR$^{-/-}$ mice also display increased fibrosis compared to controls as shown by representative picrosirius red staining (D, E). Western blotting shows a significant increase in PERK and periostin protein expression in Adipo-HuR$^{-/-}$ hearts (F-H). N > 4 per group. *P ≤ 0.05. **P ≤ 0.01.

Figure 3. Serum levels of epinephrine (A) and norepinephrine (B) as determined by ELISA. N ≥ 5 per group. **P ≤ 0.01.

Figure 4. RNA-Seq analysis of gene expression in control and Adipo-HuR$^{-/-}$ hearts. Principal component analysis (PCA) plot shows clustering of gene expression patterns from control and Adipo-HuR$^{-/-}$ hearts (A). Gene ontology (GO) analysis shows a significant enrichment in inflammation-associated genes, indicated in red (B). RNA-seq analysis shows a significant increase in hypertrophic, fibrotic, and inflammatory gene expression (C); all genes shown in panel C are significant as defined by fold change ≥ 1.5 and FDR P ≤ 0.05. N = 4 per group.

Figure 5. RNA-Seq analysis of gene expression in control and Adipo-HuR$^{-/-}$ scWAT. Venn diagram of HuR-dependent changes in gene expression changes in BAT and scWAT shows a unique set of HuR-dependent genes in the two adipose depots (A). The majority (381/588; 65%) of the significant HuR-

dependent changes in gene expression in BAT are down-regulated, while the majority (774/1117; 69%) are up-regulated in scWAT (B). Expression of beige adipocyte marker genes in scWAT (C). Gene ontology analysis showing classification by percent of all enriched HuR-dependent GO terms in scWAT (D) and the top 20 enriched HuR-dependent GO terms among genes with significantly increased expression (E). RNA-seq determined expression change of proinflammatory cytokines in scWAT that have previously been suggested to mediate cardiac pathology through secreted/paracrine signaling (F). N = 4 per group. Serum levels of TNF-α (G) and IL-6 (H) as determined by ELISA. N ≥ 5 per group. *P ≤ 0.05. **P ≤ 0.01.

Figure 6. WGCNA association of scWAT gene expression with cardiac hypertrophy phenotype. Workflow used to identify and associate co-expressed gene modules with phenotype independent of genotype (A). Gene cluster dendogram of co-expressed gene modules (B). Correlation of each gene expression module with LVW/BW was used as a first filter to identify significant modules (C). Average gene signficance relative to LVW/BW was calculated for each module as a second filter for identification of significant modules (D). (E) Confirmation of a strong significant correlation between gene significance to LVW/BW and module membership for individual genes within the three identified modules that pass both correlation (C) and average gene significance (D).

Figure 7. Enriched GO terms among genes from significant LVW/BW-associated co-expression modules. The lightsteelblue1 module (A) had exactly 10 significantly enriched GO terms. GO enrichments for the magenta module (B) represent the 10 most significantly enriched of 59 total signficant terms. The yellowgreen module (C) had only 3 significantly enriched GO terms.

Table 2. Node gene identification within significant LVW/BW associated modules.

REFERENCES

1. **Anthony SR**, **Guarnieri A**, **Ianzillotta L**, **Gozdiff A**, **Green LC**, **O'Grady K**, **Helsley RN**, **Owens AP**, **Tranter M**. HuR expression in adipose tissue mediates energy expenditure and acute thermogenesis independent of UCP1 expression. *Adipocyte* 9: 335–345, 2020.

2. **Anthony SR**, **Guarnieri AR**, **Gozdiff A**, **Helsley RN**, **Owens AP**, **Tranter M**. Mechanisms linking adipose tissue inflammation to cardiac hypertrophy and fibrosis. *Clin Sci* 133: 2329–2344, 2019.

3. **Aslibekyan S**, **Kabagambe EK**, **Irvin MR**, **Straka RJ**, **Borecki IB**, **Tiwari HK**, **Tsai MY**, **Hopkins PN**, **Shen J**, **Lai C-Q**, **Ordovas JM**, **Arnett DK**. A genome-wide association study of inflammatory biomarker changes in response to fenofibrate treatment in the Genetics of Lipid Lowering Drug and Diet Network. *Pharmacogenet Genomics* 22: 191–197, 2012.

4. **Bandstein M**, **Voisin S**, **Nilsson EK**, **Schultes B**, **Ernst B**, **Thurnheer M**, **Benedict C**, **Mwinyi J**, **Schiöth HB**. A Genetic Risk Score Is Associated with Weight Loss Following Roux-en Y Gastric Bypass Surgery. *Obes Surg* 26: 2183–2189, 2016.

5. **Bartz F**, **Kern L**, **Erz D**, **Zhu M**, **Gilbert D**, **Meinhof T**, **Wirkner U**, **Erfle H**, **Muckenthaler M**, **Pepperkok R**, **Runz H**. Identification of cholesterol-regulating genes by targeted RNAi screening. *Cell Metab* 10: 63–75, 2009.

6. **Burstein E**, **Hoberg JE**, **Wilkinson AS**, **Rumble JM**, **Csomos RA**, **Komarck CM**, **Maine GN**, **Wilkinson JC**, **Mayo MW**, **Duckett CS**. COMMD proteins, a novel family of structural and functional homologs of MURR1. *J Biol Chem* 280: 22222–22232, 2005.

7. **Busk PK**, **Wulf-Andersen L**, **Strøm CC**, **Enevoldsen M**, **Thirstrup K**, **Haunsø S**, **Sheikh SP**. Multiprotein bridging factor 1 cooperates with c-Jun and is necessary for cardiac hypertrophy in vitro. *Exp Cell Res* 286: 102–114, 2003.

8. **Cavalcanti DMLP**, **Castro LM**, **Rosa Neto JC**, **Seelaender M**, **Neves RX**, **Oliveira V**, **Forti FL**, **Iwai LK**, **Gozzo FC**, **Todiras M**, **Schadock I**, **Barros CC**, **Bader M**, **Ferro ES**. Neurolysin knockout mice generation and initial phenotype characterization. *J Biol Chem* 289: 15426–15440, 2014.

9. **Cazzaniga A**, **Locatelli L**, **Castiglioni S**, **Maier J**. The Contribution of EDF1 to PPARγ Transcriptional Activation in VEGF-Treated Human Endothelial Cells. *Int J Mol Sci* 19: 1830, 2018.

10. **Chen H**, **Zhang W**, **Sun X**, **Yoshimoto M**, **Chen Z**, **Zhu W**, **Liu J**, **Shen Y**, **Yong W**, **Li D**, **Zhang J**, **Lin Y**, **Li B**, **VanDusen NJ**, **Snider P**, **Schwartz RJ**, **Conway SJ**, **Field LJ**, **Yoder MC**, **Firulli AB**, **Carlesso N**, **Towbin JA**, **Shou W**. Fkbp1a controls ventricular myocardium trabeculation and compaction by regulating endocardial Notch1 activity. *Development* 140: 1946–1957, 2013.

11. **Choi J**, **Kim H**, **Kim Y**, **Jang M**, **Jeon J**, **Hwang Y-I**, **Shon WJ**, **Song YW**, **Kang JS**, **Lee WJ**. The Anti-inflammatory Effect of GV1001 Mediated by the Downregulation of ENO1-induced Pro-inflammatory Cytokine Production. *Immune Netw* 15: 291–303, 2015.

12. **Cypess AM**, **Lehman S**, **Williams G**, **Tal I**, **Rodman D**, **Goldfine AB**, **Kuo FC**, **Palmer EL**, **Tseng Y-H**, **Doria A**, **Kolodny GM**, **Kahn CR**. Identification and importance of brown adipose tissue in adult humans. *N Engl J Med* 360: 1509–1517, 2009.

13. **De Angelis E**, **Pecoraro M**, **Rusciano MR**, **Ciccarelli M**, **Popolo A**. Cross-Talk between Neurohormonal Pathways and the Immune System in Heart Failure: A Review of the Literature. *Int J Mol Sci* 20: 1698, 2019.

14. **Doller A**, **Pfeilschifter J**, **Eberhardt W**. Signalling pathways regulating nucleo-cytoplasmic shuttling of the mRNA-binding protein HuR. *Cell Signal* 20: 2165–2173, 2008.

15. **Dutta S**, **Roy S**, **Polavaram NS**, **Stanton MJ**, **Zhang H**, **Bhola T**, **Hönscheid P**, **Donohue TM**, **Band H**, **Batra SK**, **Muders MH**, **Datta K**. Neuropilin-2 Regulates Endosome Maturation and EGFR Trafficking to Support Cancer Cell Pathobiology. *Cancer Res* 76: 418–428, 2016.

16. **Fang C**, **Li X**, **Liang H**, **Xue L**, **Liu L**, **Yang C**, **Gao G**, **Jiang X**. Downregulation of SUMF2 gene in ovalbumin-induced rat model of allergic inflammation. *Int J Clin Exp Pathol* 8: 12053–12063, 2015.

17. **Florea S**, **Anjak A**, **Cai W-F**, **Qian J**, **Vafiadaki E**, **Figueria S**, **Haghighi K**, **Rubinstein J**, **Lorenz J**, **Kranias EG**. Constitutive phosphorylation of inhibitor-1 at Ser67 and Thr75 depresses calcium cycling in cardiomyocytes and leads to remodeling upon aging. *Basic Res Cardiol* 107: 279, 2012.

18. **Fu Y**, **Xiao H**, **Zhang Y**. Beta-adrenoceptor signaling pathways mediate cardiac pathological remodeling. *Front Biosci (Elite Ed)* 4: 1625–1637, 2012.

19. **Fuster JJ**, **Ouchi N**, **Gokce N**, **Walsh K**. Obesity-Induced Changes in Adipose Tissue Microenvironment and Their Impact on Cardiovascular Disease. *Circ Res* 118: 1786–1807, 2016.

20. **Ge Y**, **Wang L**, **Li D**, **Zhao C**, **Li J**, **Liu T**. Exploring the Extended Biological Functions of the Human Copper Chaperone of Superoxide Dismutase 1. *Protein J* 38: 463–471, 2019.

21. **Ghali R**, **Habeichi NJ**, **Kaplan A**, **Tannous C**, **Abidi E**, **Bekdash A**, **Farhat R**, **Itani H**, **Jurjus A**, **Booz GW**, **Mallat Z**, **Zouein FA**. IL-33 induces type-2-cytokine phenotype but exacerbates cardiac remodeling post-myocardial infarction with eosinophil recruitment, worsened systolic dysfunction, and ventricular wall rupture. *Clin Sci* 134: 1191–1218, 2020.

22. **Ghosh M**, **Aguila HL**, **Michaud J**, **Ai Y**, **Wu M-T**, **Hemmes A**, **Ristimaki A**, **Guo C**, **Furneaux H**, **Hla T**. Essential role of the RNA-binding protein HuR in progenitor cell survival in mice. *J Clin Invest* 119: 3530–3543, 2009.

23. **Gonano LA**, **Jones PP**. FK506-binding proteins 12 and 12.6 (FKBPs) as regulators of cardiac Ryanodine Receptors: Insights from new functional and structural knowledge. *Channels (Austin)* 11: 415–425, 2017.

24. **Green LC**, **Anthony SR**, **Slone S**, **Ianzillotta L**, **Nieman ML**, **Wu X**, **Robbins N**, **Jones SM**, **Roy S**, **Owens AP**, **Aubé J**, **Xu L**, **Lorenz JN**, **Blaxall BC**, **Rubinstein J**, **Benoit JB**, **Tranter M**. Human antigen R as a therapeutic target in pathological cardiac hypertrophy. *JCI Insight* 4: 47, 2019.

25. **Greening DW**, **Ji H**, **Chen M**, **Robinson BWS**, **Dick IM**, **Creaney J**, **Simpson RJ**. Secreted primary human malignant mesothelioma exosome signature reflects oncogenic cargo. *Sci Rep* 6: 32643–18, 2016.

26. **Gullestad L**, **Ueland T**, **Vinge LE**, **Finsen A**, **Yndestad A**, **Aukrust P**. Inflammatory cytokines in heart failure: mediators and markers. *Cardiology* 122: 23–35, 2012.

27. **Gurgis FMS**, **Yeung YT**, **Tang MXM**, **Heng B**, **Buckland M**, **Ammit AJ**, **Haapasalo J**, **Haapasalo H**, **Guillemin GJ**, **Grewal T**, **Munoz L**. The p38-MK2-HuR pathway potentiates EGFRvIII-IL-1β-driven IL-6 secretion in glioblastoma cells. *Oncogene* 34: 2934–2942, 2015.

28. **Haas BE**, **Horvath S**, **Pietiläinen KH**, **Cantor RM**, **Nikkola E**, **Weissglas-Volkov D**, **Rissanen A**, **Civelek M**, **Cruz-Bautista I**, **Riba L**, **Kuusisto J**, **Kaprio J**, **Tusie-Luna T**, **Laakso M**, **Aguilar-Salinas CA**, **Pajukanta P**. Adipose co-expression networks across Finns and Mexicans identify novel triglyceride-associated genes. *BMC Med Genomics* 5: 61–10, 2012.

29. **Hadi AM**, **Mouchaers KTB**, **Schalij I**, **Grunberg K**, **Meijer GA**, **Vonk-Noordegraaf A**, **van der Laarse WJ**, **Beliën JAM**. Rapid quantification of myocardial fibrosis: a new macro-based automated analysis. *Cell Oncol* 34: 343–354, 2011.

30. **Heimann AS**, **Favarato MH**, **Gozzo FC**, **Rioli V**, **Carreño FR**, **Eberlin MN**, **Ferro ES**, **Krege JH**, **Krieger JE**. ACE gene titration in mice uncovers a new mechanism for ACE on the control of body weight. *Physiol Genomics* 20: 173–182, 2005.

31. **Hong J**, **Shi J**, **Qi L**, **Cui B**, **Gu W**, **Zhang Y**, **Li L**, **Xu M**, **Wang L**, **Zhai Y**, **Miao L**, **Wang R**, **Bi Y**, **Wang W**, **Ning G**. Genetic susceptibility, birth weight and obesity risk in young Chinese. *Int J Obes (Lond)* 37: 673–677, 2013.

32. **Howson JMM**, **Walker NM**, **Smyth DJ**, **Todd JA**, **Type I Diabetes Genetics Consortium**. Analysis of 19 genes for association with type I diabetes in the Type I Diabetes Genetics Consortium families. *Genes Immun* 10 Suppl 1: S74–84, 2009.

33. **Hsiao K-C**, **Shih N-Y**, **Fang H-L**, **Huang T-S**, **Kuo C-C**, **Chu P-Y**, **Hung Y-M**, **Chou S-W**, **Yang Y-Y**, **Chang G-C**, **Liu K-J**. Surface α-enolase promotes extracellular matrix degradation and tumor metastasis and represents a new therapeutic target. *PLoS ONE* 8: e69354, 2013.

34. **Hu Y-H**, **Zhang Y**, **Jiang L-Q**, **Wang S**, **Lei C-Q**, **Sun M-S**, **Shu H-B**, **Liu Y**. WDFY1 mediates TLR3/4 signaling by recruiting TRIF. *EMBO Rep* 16: 447–455, 2015.

35. **Huang DW**, **Sherman BT**, **Lempicki RA**. Systematic and integrative analysis of large gene lists using DAVID bioinformatics resources. *Nat Protoc* 4: 44–57, 2009.

36. **Huang DW**, **Sherman BT**, **Lempicki RA**. Bioinformatics enrichment tools: paths toward the comprehensive functional analysis of large gene lists. *Nucleic Acids Res* 37: 1–13, 2009.

37. **Jensen BC**, **Bultman SJ**, **Holley D**, **Tang W**, **de Ridder G**, **Pizzo S**, **Bowles D**, **Willis MS**. Upregulation of autophagy genes and the unfolded protein response in human heart failure. *Int J Clin Exp Med* 10: 1051–1058, 2017.

38. **Jian Z**, **Liang B**, **Pan X**, **Xu G**, **Guo S-S**, **Li T**, **Zhou T**, **Xiao Y-B**, **Li A-L**. CUEDC2 modulates cardiomyocyte oxidative capacity by regulating GPX1 stability. *EMBO Mol Med* 8: 813–829, 2016.

39. **Jiang K**, **Dong C**, **Yin Z**, **Li R**, **Mao J**, **Wang C**, **Zhang J**, **Gao Z**, **Liang R**, **Wang Q**, **Wang L**. Exosome-derived ENO1 regulates integrin α6β4 expression and promotes hepatocellular carcinoma growth and metastasis. *Cell Death Dis* 11: 972–20, 2020.

40. **Jin W**, **Jin W**, **Pan D**. Ifi27 is indispensable for mitochondrial function and browning in adipocytes. *Biochem Biophys Res Commun* 501: 273–279, 2018.

41. **Jo DH**, **Lee JH**, **Jun HJ**, **Kim J**, **Wen Q**, **Hoang MH**, **Yu YS**, **Kim JH**, **Lee SJ**. Gene expression profiles of primary retinal pigment epithelial cells from apolipoprotein E knockout and human apolipoprotein E2 transgenic mice. *Genet Mol Res* 14: 1855–1867, 2015.

42. **Katsanou V**, **Papadaki O**, **Milatos S**, **Blackshear PJ**, **Anderson P**, **Kollias G**, **Kontoyiannis DL**. HuR as a negative posttranscriptional modulator in inflammation. *Mol Cell* 19: 777–789, 2005.

43. **Kim J-W**, **Oh S-H**, **Lee MN**, **Song JH**, **Jeong B-C**, **Yang J-W**, **Piao X**, **Zang Y**, **Ryu J-H**, **Koh J-T**. CUEDC2 controls osteoblast differentiation and bone formation via SOCS3-STAT3 pathway. *Cell Death Dis* 11: 344–13, 2020.

44. **Kim Y**, **Noren Hooten N**, **Dluzen DF**, **Martindale JL**, **Gorospe M**, **Evans MK**. Post-transcriptional regulation of the inflammatory marker C-reactive protein by the RNA-binding protein HuR and miR-637. *Mol. Cell. Biol.* (October 5, 2015). doi: 10.1128/MCB.00645-15.

45. **Kolos JM**, **Voll AM**, **Bauder M**, **Hausch F**. FKBP Ligands-Where We Are and Where to Go? *Front Pharmacol* 9: 1425, 2018.

46. **Langfelder P**, **Horvath S**. WGCNA: an R package for weighted correlation network analysis. *BMC Bioinformatics* 9: 559–13, 2008.

47. **Li F**, **Tang C**, **Jin D**, **Guan L**, **Wu Y**, **Liu X**, **Wu X**, **Wu QY**, **Gao D**. CUEDC2 suppresses glioma tumorigenicity by inhibiting the activation of STAT3 and NF-κB signaling pathway. *Int J Oncol* 51: 115–127, 2017.

48. **Li J**, **Gong L**, **Liu S**, **Zhang Y**, **Zhang C**, **Tian M**, **Lu H**, **Bu P**, **Yang J**, **Ouyang C**, **Jiang X**, **Wu J**, **Zhang Y**, **Min Q**, **Zhang C**, **Zhang W**. Adipose HuR protects against diet-induced obesity and insulin resistance. *Nat Commun* 10: 2375–12, 2019.

49. **Liang H**, **Li Z**, **Xue L**, **Jiang X**, **Liu F**. SUMF2 interacts with interleukin-13 and inhibits interleukin-13 secretion in bronchial smooth muscle cells. *J Cell Biochem* 108: 1076–1083, 2009.

50. **Liu N**, **Zuo C**, **Wang X**, **Chen T**, **Yang D**, **Wang J**, **Zhu H**. miR-942 decreases TRAIL-induced apoptosis through ISG12a downregulation and is regulated by AKT. *Oncotarget* 5: 4959–4971, 2014.

51. **Lorenz JN**. A practical guide to evaluating cardiovascular, renal, and pulmonary function in mice. *Am J Physiol Regul Integr Comp Physiol* 282: R1565–82, 2002.

52. **López-Victorio CJ**, **Velez-delValle C**, **Beltrán-Langarica A**, **Kuri-Harcuch W**. EDF-1 downregulates the CaM/Cn/NFAT signaling pathway during adipogenesis. *Biochem Biophys Res Commun* 432: 146–151, 2013.

53. **Man J**, **Zhang X**. CUEDC2: an emerging key player in inflammation and tumorigenesis. *Protein Cell* 2: 699–703, 2011.

54. **McGourty CA**, **Akopian D**, **Walsh C**, **Gorur A**, **Werner A**, **Schekman R**, **Bautista D**, **Rape M**. Regulation of the CUL3 Ubiquitin Ligase by a Calcium-Dependent Co-adaptor. *Cell* 167: 525–538.e14, 2016.

55. **McLaughlin T**, **Lamendola C**, **Liu A**, **Abbasi F**. Preferential fat deposition in subcutaneous versus visceral depots is associated with insulin sensitivity. *J Clin Endocrinol Metab* 96: E1756–60, 2011.

56. **Meléndez GC**, **McLarty JL**, **Levick SP**, **Du Y**, **Janicki JS**, **Brower GL**. Interleukin 6 mediates myocardial fibrosis, concentric hypertrophy, and diastolic dysfunction in rats. *Hypertension* 56: 225–231, 2010.

57. **Mishra SK**, **Gao Y-G**, **Zou X**, **Stephenson DJ**, **Malinina L**, **Hinchcliffe EH**, **Chalfant CE**, **Brown RE**. Emerging roles for human glycolipid transfer protein superfamily members in the regulation of autophagy, inflammation, and cell death. *Prog Lipid Res* 78: 101031, 2020.

58. **Mouhadeb O**, **Ben Shlomo S**, **Cohen K**, **Farkash I**, **Gruber S**, **Maharshak N**, **Halpern Z**, **Burstein E**, **Gluck N**, **Varol C**. Impaired COMMD10-Mediated Regulation of Ly6Chi Monocyte-Driven Inflammation Disrupts Gut Barrier Function. *Front Immunol* 9: 2623, 2018.

59. **Neeland IJ**, **Poirier P**, **Després J-P**. Cardiovascular and Metabolic Heterogeneity of Obesity: Clinical Challenges and Implications for Management. *Circulation* 137: 1391–1406, 2018.

60. **Neumüller O**, **Hoffmeister M**, **Babica J**, **Prelle C**, **Gegenbauer K**, **Smolenski AP**. Synaptotagmin-like protein 1 interacts with the GTPase-activating protein Rap1GAP2 and regulates dense granule secretion in platelets. *Blood* 114: 1396–1404, 2009.

61. **Pan D**, **Chen J**, **Feng C**, **Wu W**, **Wang Y**, **Tong J**, **Zhou D**. Preferential Localization of MUC1 Glycoprotein in Exosomes Secreted by Non-Small Cell Lung Carcinoma Cells. *Int J Mol Sci* 20: 323, 2019.

62. **Papaioannou A**, **Higa A**, **Jégou G**, **Jouan F**, **Pineau R**, **Saas L**, **Avril T**, **Pluquet O**, **Chevet E**. Alterations of EDEM1 functions enhance ATF6 pro-survival signaling. *FEBS J* 285: 4146–4164, 2018.

63. **Pinckard KM**, **Shettigar VK**, **Wright KR**, **Abay E**, **Baer LA**, **Vidal P**, **Dewal RS**, **Das D**, **Duarte-Sanmiguel S**, **Hernández-Saavedra D**, **Arts PJ**, **Lehnig AC**, **Bussberg V**, **Narain NR**, **Kiebish MA**, **Yi F**, **Sparks LM**, **Goodpaster BH**, **Smith SR**, **Pratley RE**, **Lewandowski ED**, **Raman SV**, **Wold LE**, **Gallego-Perez D**, **Coen PM**, **Ziolo MT**, **Stanford KI**. A Novel Endocrine Role the BAT-Released Lipokine 12,13-diHOME to Mediate Cardiac Function. *Circulation* 139: e56, 2020.

64. **Riad A**, **Zeng C**, **Weng C-C**, **Winters H**, **Xu K**, **Makvandi M**, **Metz T**, **Carlin S**, **Mach RH**. Sigma-2 Receptor/TMEM97 and PGRMC-1 Increase the Rate of Internalization of LDL by LDL Receptor through the Formation of a Ternary Complex. *Sci Rep* 8: 16845–12, 2018.

65. **Rolfe DF**, **Brown GC**. Cellular energy utilization and molecular origin of standard metabolic rate in mammals. *Physiol Rev* 77: 731–758, 1997.

66. **Rosebeck S**, **Leaman DW**. Mitochondrial localization and pro-apoptotic effects of the interferon-inducible protein ISG12a. *Apoptosis* 13: 562–572, 2008.

67. **Schlager MA**, **Kapitein LC**, **Grigoriev I**, **Burzynski GM**, **Wulf PS**, **Keijzer N**, **de Graaff E**, **Fukuda M**, **Shepherd IT**, **Akhmanova A**, **Hoogenraad CC**. Pericentrosomal targeting of Rab6 secretory vesicles by Bicaudal-D-related protein 1 (BICDR-1) regulates neuritogenesis. *EMBO J* 29: 1637–1651, 2010.

68. **Schultess J**, **Danielewski O**, **Smolenski AP**. Rap1GAP2 is a new GTPase-activating protein of Rap1 expressed in human platelets. *Blood* 105: 3185–3192, 2005.

69. **Siang DTC**, **Lim YC**, **Kyaw AMM**, **Win KN**, **Chia SY**, **Degirmenci U**, **Hu X**, **Tan BC**, **Walet ACE**, **Sun L**, **Xu D**. The RNA-binding protein HuR is a negative regulator in adipogenesis. *Nat Commun* 11: 213–13, 2020.

70. **Slone S**, **Anthony SR**, **Wu X**, **Benoit JB**, **Aubé J**, **Xu L**, **Tranter M**. Activation of HuR downstream of p38 MAPK promotes cardiomyocyte hypertrophy. *Cell Signal* 28: 1735–1741, 2016.

71. **Srikantan S**, **Gorospe M**. HuR function in disease. *Front Biosci (Landmark Ed)* 17: 189–205, 2012.

72. **Stanford KI**, **Middelbeek RJW**, **Townsend KL**, **An D**, **Nygaard EB**, **Hitchcox KM**, **Markan KR**, **Nakano K**, **Hirshman MF**, **Tseng Y-H**, **Goodyear LJ**. Brown adipose tissue regulates glucose homeostasis and insulin sensitivity. *J Clin Invest* 123: 215–223, 2013.

73. **Tamaki S**, **Mano T**, **Sakata Y**, **Ohtani T**, **Takeda Y**, **Kamimura D**, **Omori Y**, **Tsukamoto Y**, **Ikeya Y**, **Kawai M**, **Kumanogoh A**, **Hagihara K**, **Ishii R**, **Higashimori M**, **Kaneko M**, **Hasuwa H**, **Miwa T**, **Yamamoto K**, **Komuro I**. Interleukin-16 promotes cardiac fibrosis and myocardial stiffening in heart failure with preserved ejection fraction. *PLoS ONE* 8: e68893, 2013.

74. **Thoonen R**, **Ernande L**, **Cheng J**, **Nagasaka Y**, **Yao V**, **Miranda-Bezerra A**, **Chen C**, **Chao W**, **Panagia M**, **Sosnovik DE**, **Puppala D**, **Armoundas AA**, **Hindle A**, **Bloch KD**, **Buys ES**, **Scherrer-Crosbie M**. Functional brown adipose tissue limits cardiomyocyte injury and adverse remodeling in catecholamine-induced cardiomyopathy. *J Mol Cell Cardiol* 84: 202–211, 2015.

75. **Thyagarajan B**, **Foster MT**. Beiging of white adipose tissue as a therapeutic strategy for weight loss in humans. *Horm Mol Biol Clin Investig* 31: 1500, 2017.

76. **Townsend K**, **Tseng Y-H**. Brown adipose tissue: Recent insights into development, metabolic function and therapeutic potential. *Adipocyte* 1: 13–24, 2012.

77. **Tranter M**, **Ren X**, **Forde T**, **Wilhide ME**, **Chen J**, **Sartor MA**, **Medvedovic M**, **Jones WK**. NF-kappaB driven cardioprotective gene programs; Hsp70.3 and cardioprotection after late ischemic preconditioning. *J Mol Cell Cardiol* 49: 664–672, 2010.

78. **Tsunematsu T**, **Yamauchi E**, **Shibata H**, **Maki M**, **Ohta T**, **Konishi H**. Distinct functions of human MVB12A and MVB12B in the ESCRT-I dependent on their posttranslational modifications. *Biochem Biophys Res Commun* 399: 232–237, 2010.

79. **Valcz G**, **Galamb O**, **Krenács T**, **Spisák S**, **Kalmár A**, **Patai ÁV**, **Wichmann B**, **Dede K**, **Tulassay Z**, **Molnár B**. Exosomes in colorectal carcinoma formation: ALIX under the magnifying glass. *Mod Pathol* 29: 928–938, 2016.

80. **van Marken Lichtenbelt WD**, **Vanhommerig JW**, **Smulders NM**, **Drossaerts JMAFL**, **Kemerink GJ**, **Bouvy ND**, **Schrauwen P**, **Teule GJJ**. Cold-activated brown adipose tissue in healthy men. *N Engl J Med* 360: 1500–1508, 2009.

81. **Wang M**, **Wang J**, **Liu J**, **Zhu L**, **Ma H**, **Zou J**, **Wu W**, **Wang K**. Systematic prediction of key genes for ovarian cancer by co-expression network analysis. *J Cell Mol Med* 24: 6298–6307, 2020.

82. **Wang T**, **Donahoe PK**. The immunophilin FKBP12: a molecular guardian of the TGF-beta family type I receptors. *Front Biosci* 9: 619–631, 2004.

83. **Wang X**, **Duanmu J**, **Fu X**, **Li T**, **Jiang Q**. Analyzing and validating the prognostic value and mechanism of colon cancer immune microenvironment. *J Transl Med* 18: 324–14, 2020.

84. **Ware AW**, **Cheung TT**, **Rasulov S**, **Burstein E**, **McDonald FJ**. Epithelial Na+ Channel: Reciprocal Control by COMMD10 and Nedd4-2. *Front Physiol* 9: 793, 2018.

85. **Wen J**, **Ma Z**, **Livingston MJ**, **Zhang W**, **Yuan Y**, **Guo C**, **Liu Y**, **Fu P**, **Dong Z**. Decreased secretion and profibrotic activity of tubular exosomes in diabetic kidney disease. *AJP: Renal Physiology* 319: F664–F673, 2020.

86. **Yang SS**, **Li XM**, **Yang M**, **Ren XL**, **Hu JL**, **Zhu XH**, **Wang FF**, **Zeng ZC**, **Li JY**, **Cheng ZQ**, **Liao WT**, **Ding YQ**, **Guan J**, **Liang L**. FMNL2 destabilises COMMD10 to activate NF-κB pathway in invasion and metastasis of colorectal cancer. *Br J Cancer* 117: 1164–1175, 2017.

87. **Yiakouvaki A**, **Dimitriou M**, **Karakasiliotis I**, **Eftychi C**, **Theocharis S**, **Kontoyiannis DL**. Myeloid cell expression of the RNA-binding protein HuR protects mice from pathologic inflammation and colorectal carcinogenesis. *J Clin Invest* 122: 48–61, 2012.

88. **Yuan Y**, **Wang Y**, **Liu Z**, **Sun Y**, **Yao Y**, **Yu W**, **Shen Z**. MAT2B promotes proliferation and inhibits apoptosis in osteosarcoma by targeting epidermal growth factor receptor and proliferating cell nuclear antigen. *Int J Oncol* 54: 2019–2029, 2019.

89. **Zhang B**, **Horvath S**. A general framework for weighted gene co-expression network analysis. *Stat Appl Genet Mol Biol* 4: Article17, 2005.

90. **Zhang G**, **Wang X**, **Gillette TG**, **Deng Y**, **Wang ZV**. Unfolded Protein Response as a Therapeutic Target in Cardiovascular Disease. *CTMC* 19: 1902–1917, 2019.

91. **Zhao C**, **Chen X**, **Wu W**, **Wang W**, **Pang W**, **Yang G**. MAT2B promotes adipogenesis by modulating SAMe levels and activating AKT/ERK pathway during porcine intramuscular preadipocyte differentiation. *Exp Cell Res* 344: 11–21, 2016.

92. **Zhao L**, **Cheng G**, **Jin R**, **Afzal MR**, **Samanta A**, **Xuan Y-T**, **Girgis M**, **Elias HK**, **Zhu Y**, **Davani A**, **Yang Y**, **Chen X**, **Ye S**, **Wang O-L**, **Chen L**, **Hauptman J**, **Vincent RJ**, **Dawn B**. Deletion of Interleukin-6 Attenuates Pressure Overload-Induced Left Ventricular Hypertrophy and Dysfunction. *Circ Res* 118: 1918–1929, 2016.

93. **Zheng N**, **Wei D**, **Dai B**, **Zheng L**, **Zhao M**, **Xin N**, **Chi Z**, **Zhao Y**, **Ma T**, **Jahane R**, **Sun L**. Mitochondrial Genome Encoded Proteins Expression Disorder, the Possible Mechanism of the Heart Disease in Metabolic Syndrome. *Cell Physiol Biochem* 43: 959–968, 2017.

Fig. 1. Adipocyte-specific deletion of HuR induces a state of hypercontractility and hypertrophy.

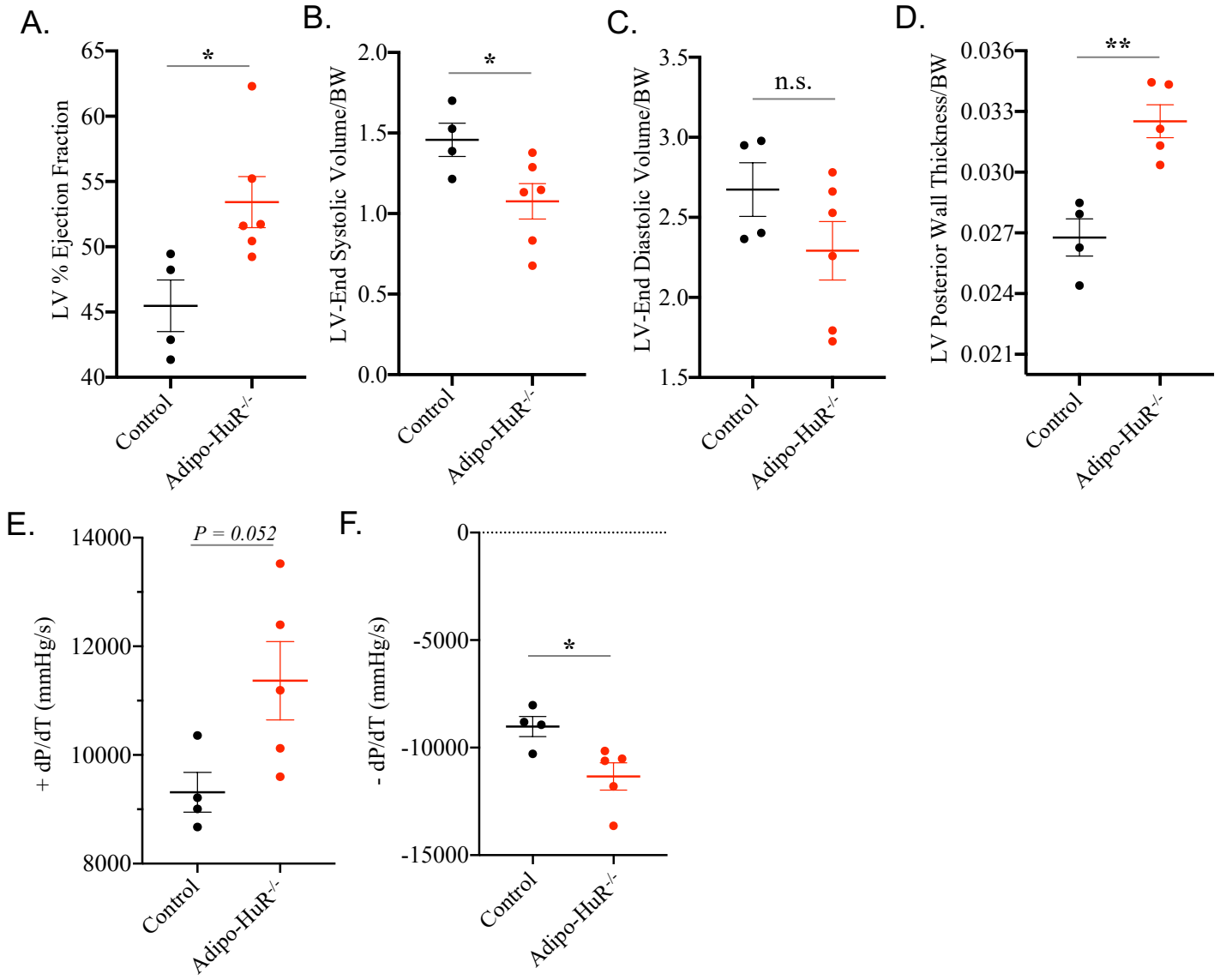

Fig. 2. Molecular assessment of cardiac hypertrophy and fibrosis.

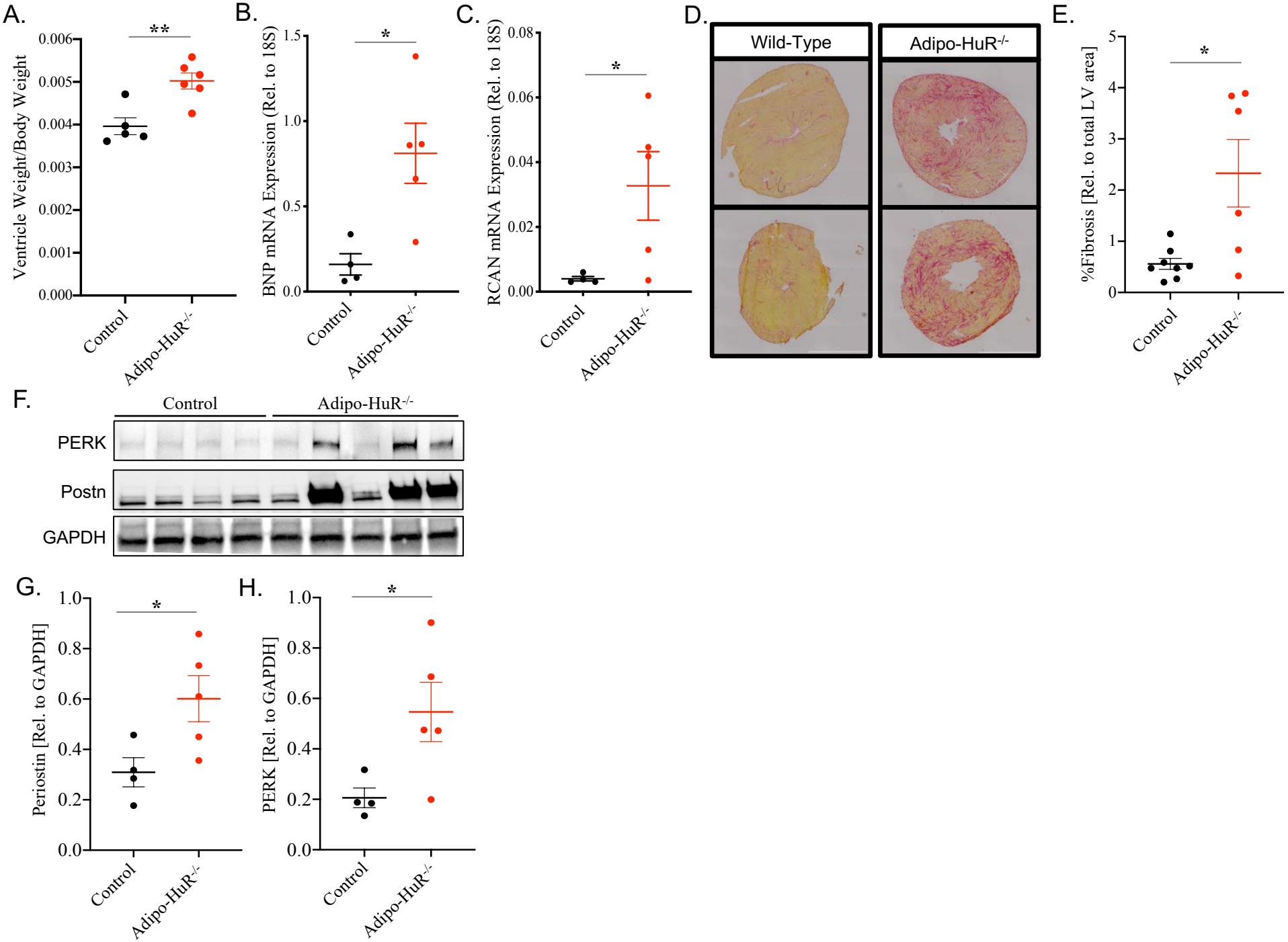

Fig. 3. Cardiac remodeling in Adipo-HuR$^{-/-}$ mice is not due to increased catecholamines.

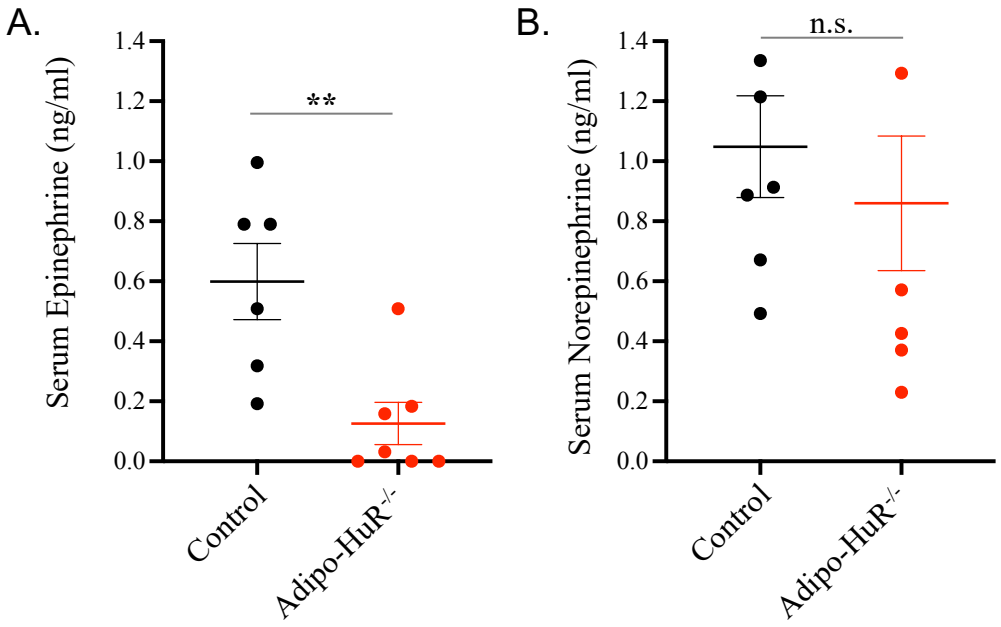

Fig. 4. RNA-Seq analysis shows increased inflammatory gene expression in Adipo-HuR$^{-/-}$ hearts.

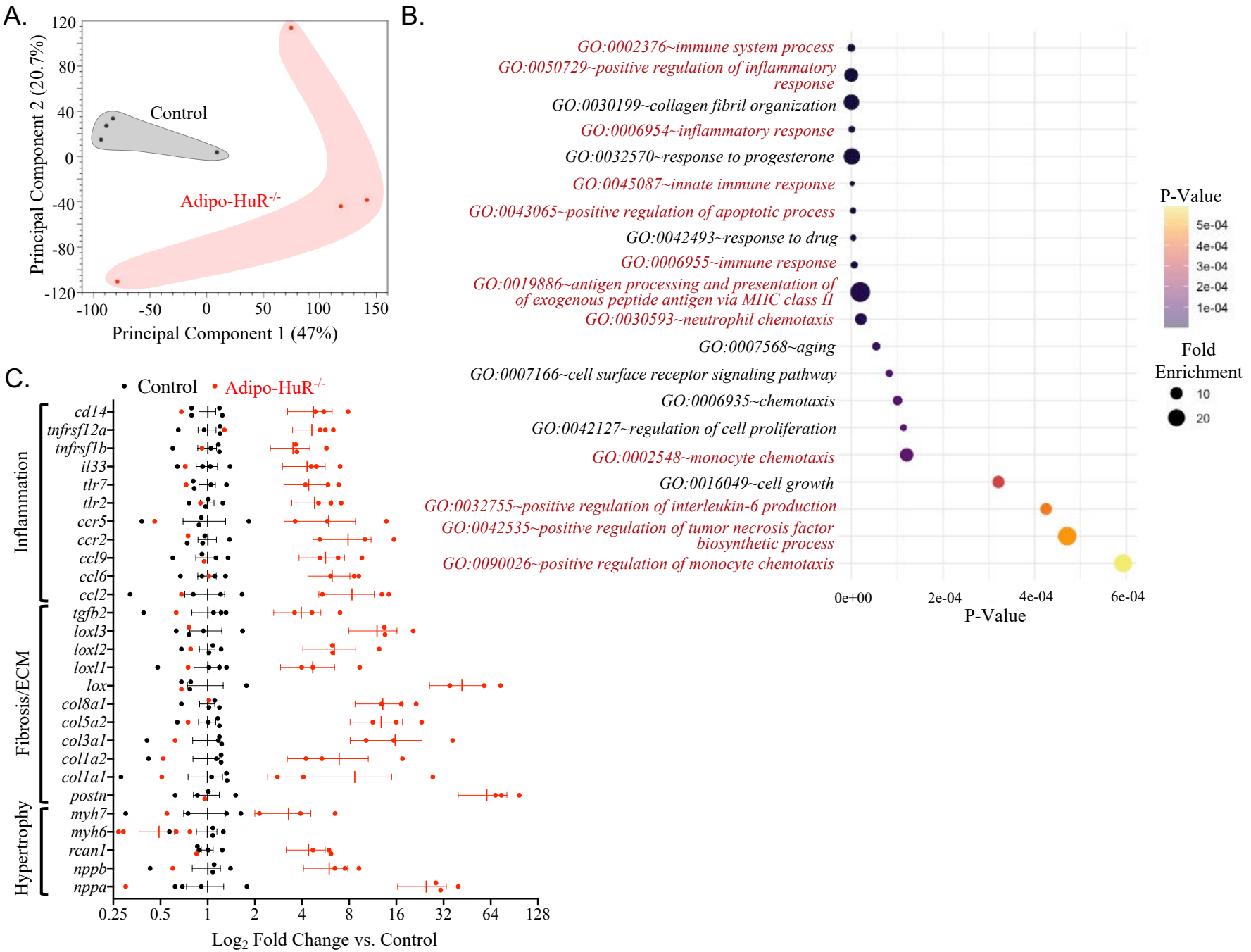

Fig. 5. Adipo-HuR$^{-/-}$ mice have increased pro-inflammatory gene expression in scWAT.

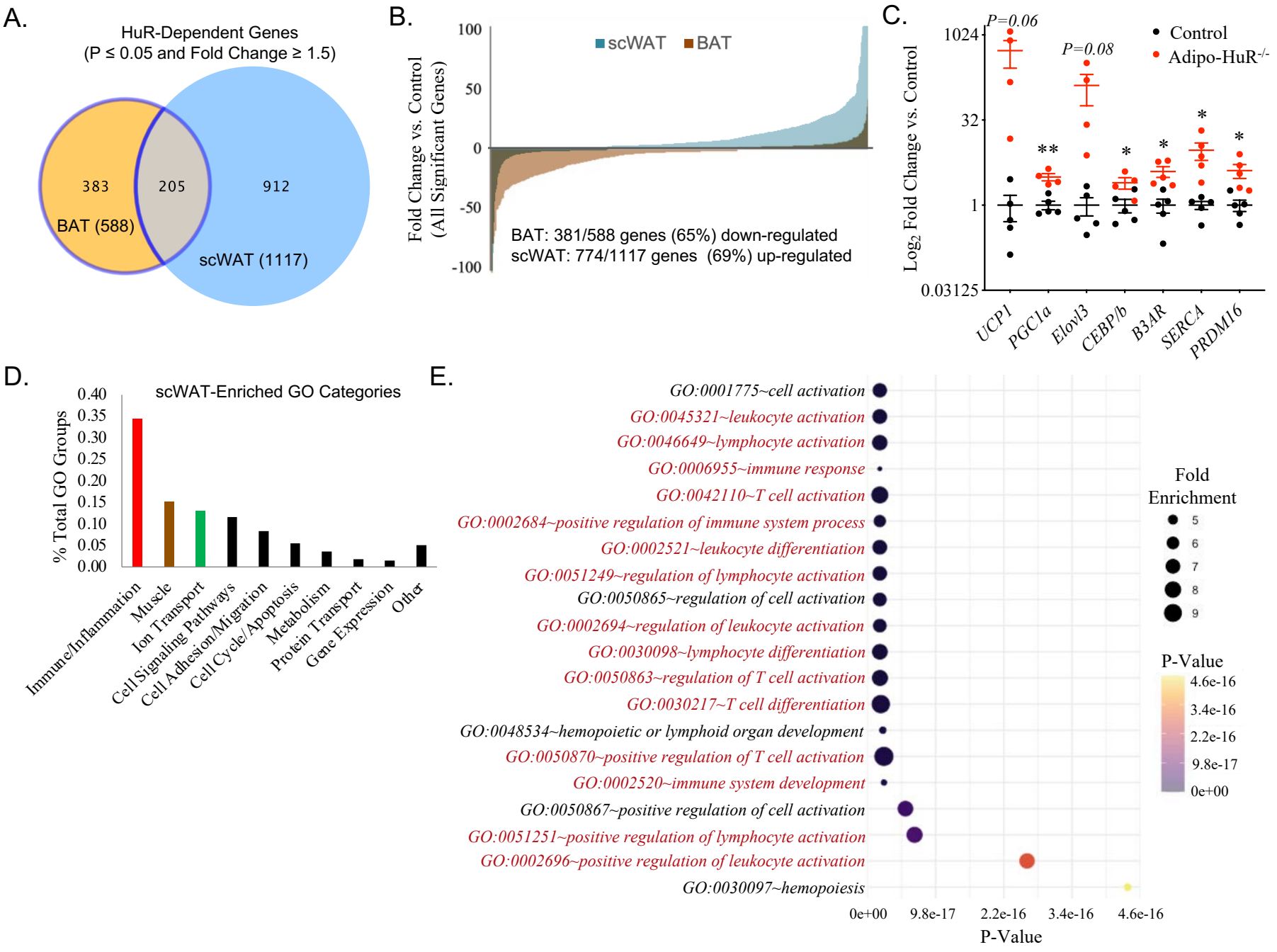

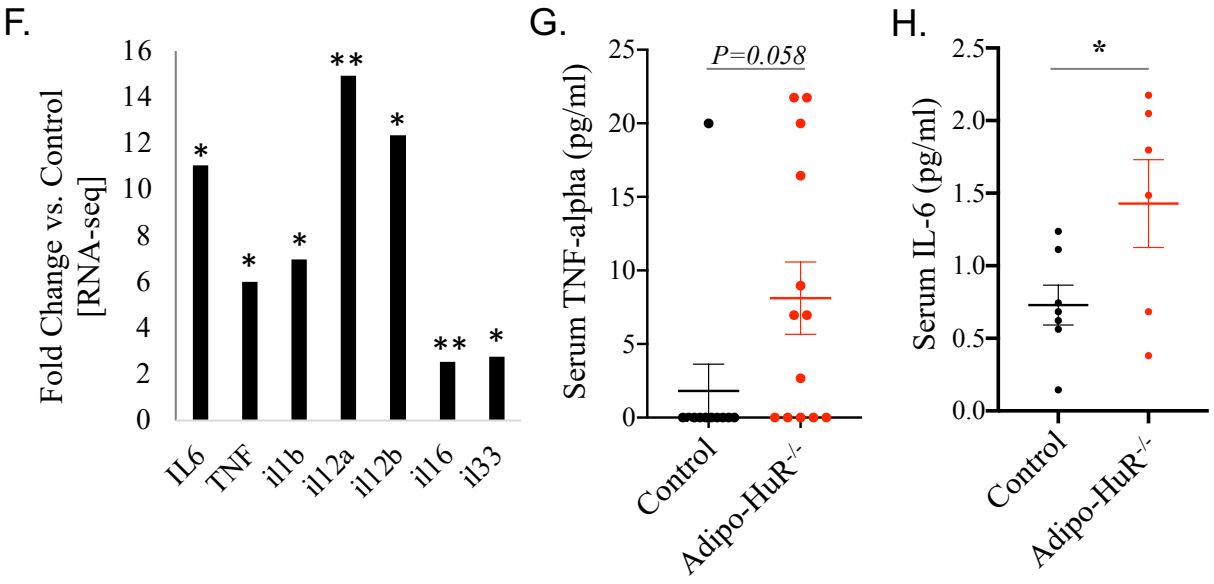
F.
Fold Change vs. Control [RNA-seq]
16
14
12
10
8
6
4
2
0
*
*
*
**
*
**
*
IL6
TNF
il1b
il12a
il12b
il16
il33
G.
Serum TNF-alpha (pg/ml)
25
20
15
10
5
0
P=0.058
Control
Adipo-HuR-/-
H.
Serum IL-6 (pg/ml)
2.5
2.0
1.5
1.0
0.5
0.0
*
Control
Adipo-HuR-/-

Fig. 6. WGCNA association of scWAT gene expression with cardiac hypertrophy phenotype.

A.

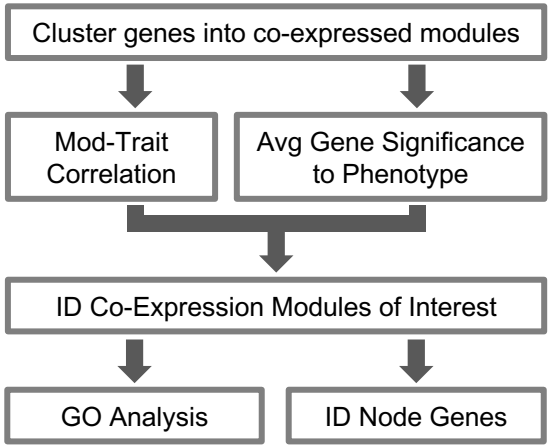

B.

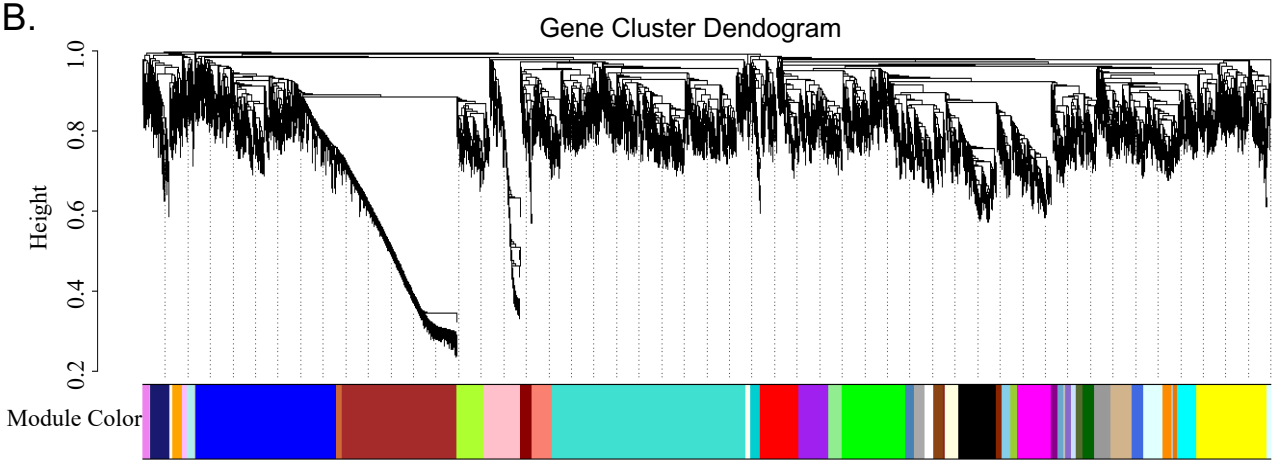

C.

Module	LVW/BW	Module	LVW/BW
blue	0.69 (0.04)	orangered4	-0.8 (0.01)
ivory	-0.72 (0.03)	paleturquoise	-0.75 (0.02)
lightcyan	-0.69 (0.04)	pink	-0.83 (0.006)
lightgreen	-0.7 (0.03)	purple	-0.77 (0.02)
lightsteelblue1	-0.79 (0.01)	turquoise	-0.73 (0.02)
lightyellow	-0.75 (0.02)	violet	-0.78 (0.01)
magenta	-0.85 (0.004)	white	-0.71 (0.03)
mediumpurple3	-0.7 (0.03)	yellow	-0.87 (0.002)
midnightblue	-0.73 (0.03)	yellowgreen	-0.73 (0.02)
orange	-0.86 (0.003)		

D.

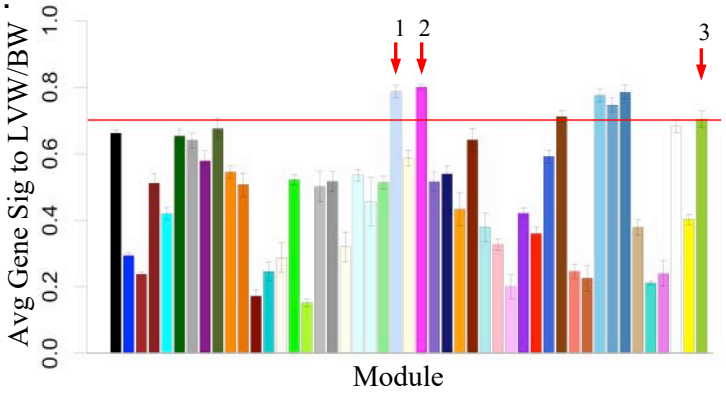

E.

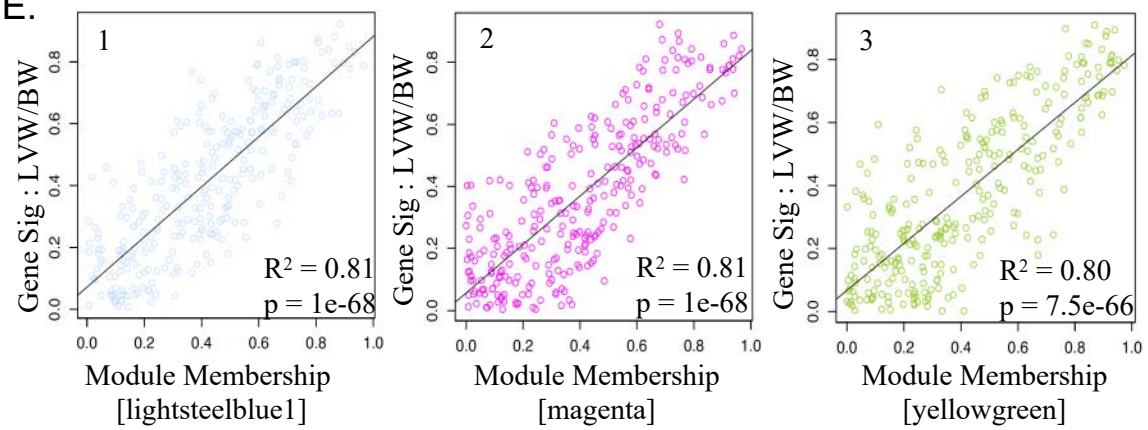

Figure 7. Enriched GO Terms from significant LVW/BW associated co-expression modules.

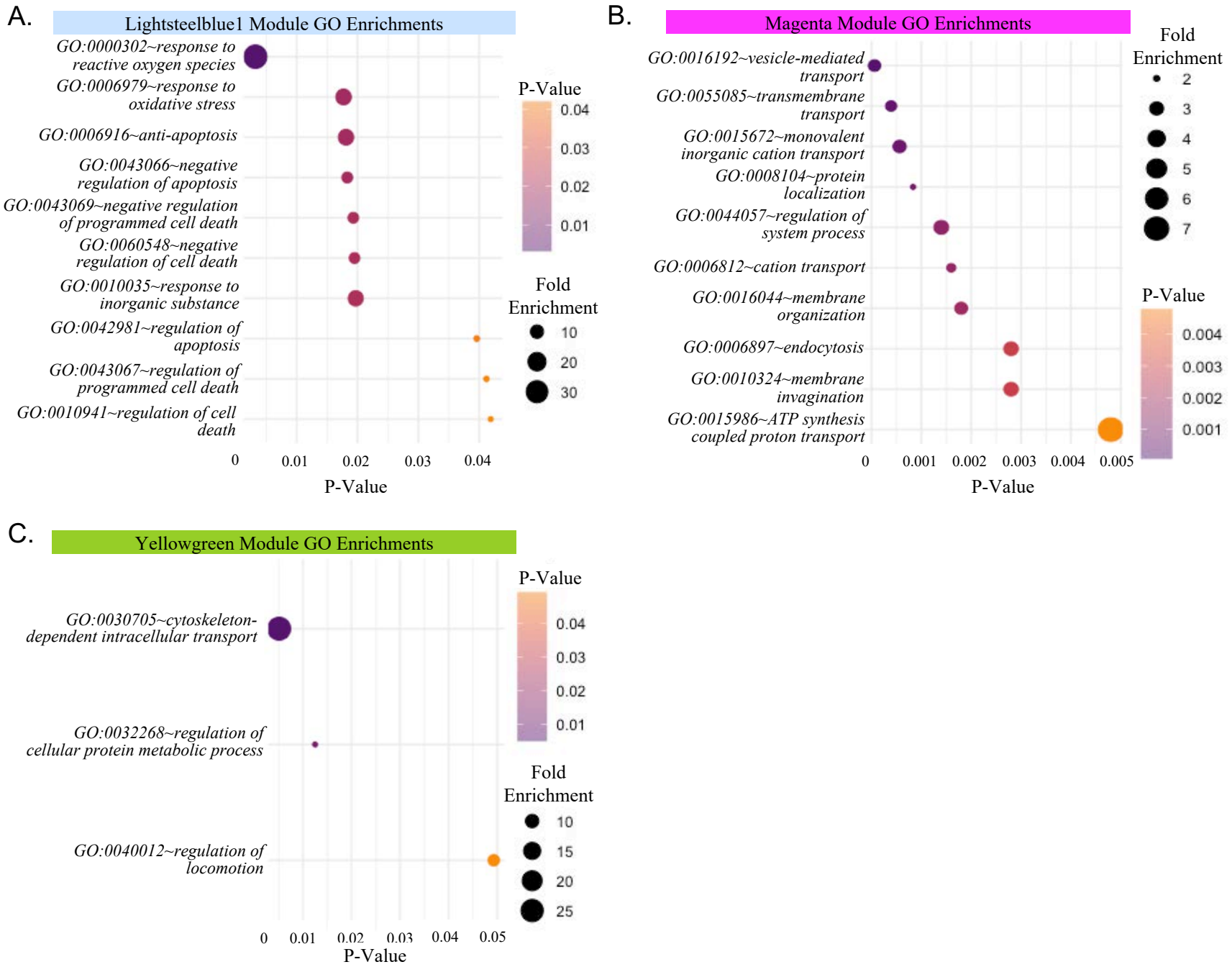

Table 1. Node gene identification significant LVW/BW associated modules.

lightsteelblue1

Symbol	Gene Sig LVW/BW	P-value	Relevant Biological Function
mat2b	0.9242	0.0004	Adipogenesis (1); Proliferation/Anti-apoptosis (2)
sumf2	0.8968	0.0011	IL-13 expression and secretion (3, 4)
cuedc2	0.8895	0.0013	Inflammatory signaling (5, 6, 7); myocardial I/R injury and oxidative stress (8)
wdfy1	0.8819	0.0017	TLR4 signaling (9); Endosome trafficking (10)
mrpl27	0.8708	0.0022	Experimental correlation with CVD in metabolic syndrome (11)
pef1	0.8693	0.0023	Ca-dependent ER-Golgi transport and collagen export (12)
edf1	0.8620	0.0028	Lipid metabolism (13); Myocyte hypertrophy (14); CaM/NFAT signaling during adipogenesis (15); PPARgamma transcriptional cofactor (16)
tmem160	0.8577	0.0031	Unknown; Clinical association with obesity risk (17, 18)
edem1	0.8539	0.0034	ATF6-mediated cell survival ER stress response (19)
ifi27	0.8503	0.0037	IFN-gamma mediated apoptosis (20-22)

magenta

Gene	Gene Sig LVW/BW	P-value	Relevant Biological Function
Atp6v1c2	0.95	0.0001	Acidification of intracellular compartements
Pigs	0.95	0.0001	Biosynthesis of glycolipid cell surface anchor
Eno1	0.94	0.0002	Identified in extracellular vesicles/exosomes (23-27); Promotes ECM degradation (28) and inflammation (29)
Gltp	0.93	0.0003	Vesicular trafficking, sphingolipid homeostasis, necroptosis (30)
Rap1gap2	0.92	0.0004	RAP1 GTPase signaling (31); Dense granule secretion in platelets (32)
Tmem254c	0.92	0.0004	Unknown
Vldlr	0.91	0.0007	Receptor-mediated endocytosis
Commd10	0.91	0.0005	NF-kappaB signaling (33, 34); Endocytosis (35); Ly6C(hi) monocyte inflammasome activity (36); Clinical GWAS correlation with inflammatory biomarkers (37)
Fkbp1a	0.89	0.0012	TGF-beta signaling (38); Ryanadine receptor-mediated calcium transport (39); Left ventricular non-compaction (40); Immunosuppresent in complex with rapamycin (41)
Nln	0.88	0.0015	Glucose tolerance/insulin sensitivity (42); Adipose expression associated with angiotensin-mediated weight gain (43)

yellowgreen

Gene	Gene Sig LVW/BW	P-value	Relevant Biological Function
Bicdl1	0.91	0.0006	Regulates secretory vesicle transport (44)
Tmem62	0.91	0.0007	Unknown
Tmem97	0.89	0.0014	LDLR endocytosis (45); Cellular cholesterol homeostasis (46)
Mvb12b	0.87	0.0022	Mediates sorting of ubiquitinated proteins to endosomal vesicles (47)
Oas1c	0.86	0.0029	SNP associated with diabetes susceptibility (48)
Ccs	0.86	0.0030	Copper homeostasis and oxidative stress (49)